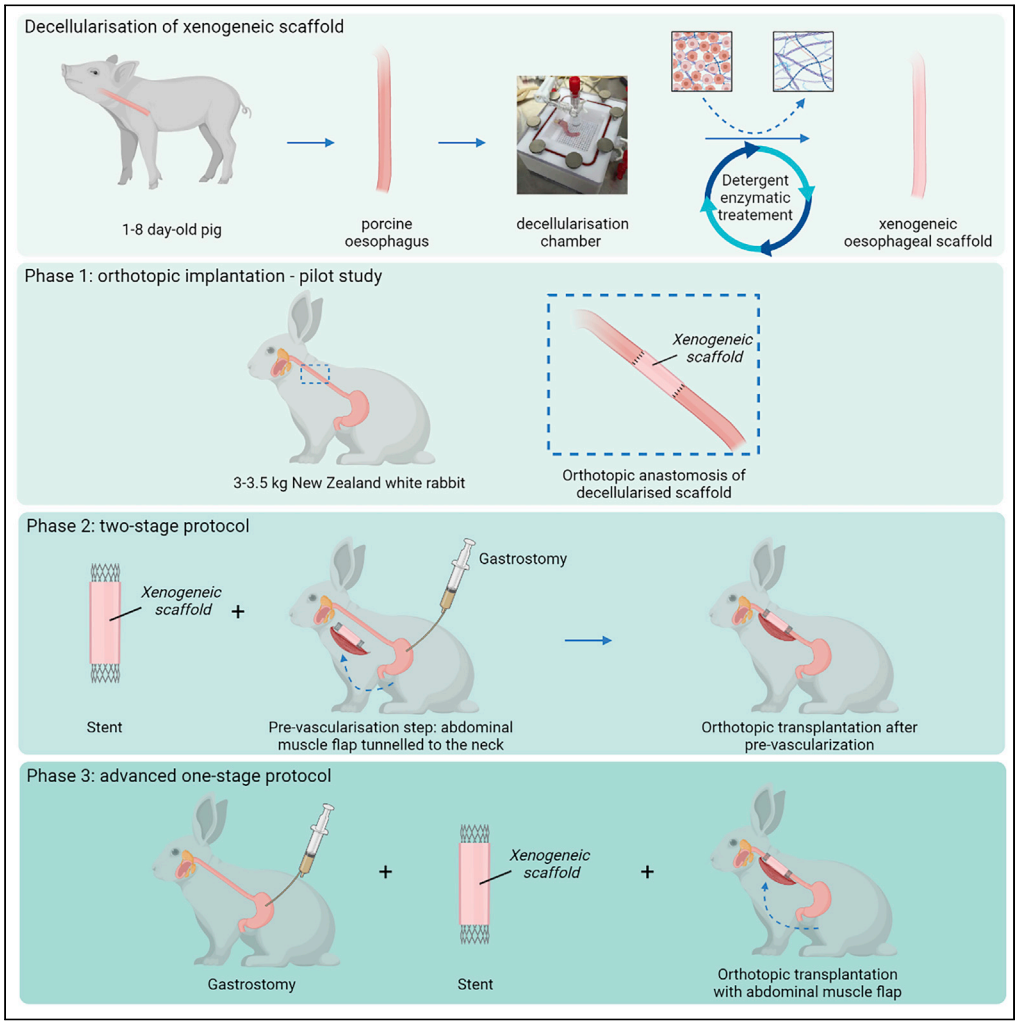
iScience

CellPress
OPEN ACCESS

Article

Lessons learned from pre-clinical testing of xenogeneic decellularized esophagi in a rabbit model



Edward Hannon, Marco Pellegrini, Federico Scottoni, ..., Paola Bonfanti, Luca Urbani, Paolo De Coppi

p.decoppi@ucl.ac.uk

Highlights

Decellularized porcine esophageal scaffold can be transplanted in rabbits

Abdominal muscle flap supports neovascularization of a porcine esophageal scaffold

Biodegradable stents support luminal patency preventing scaffold collapse

Rabbits are a poor model to study long-term outcomes of esophageal replacement

Hannon et al., iScience 25, 105174
October 21, 2022 © 2022
https://doi.org/10.1016/j.isci.2022.105174

iScience

CellPress
OPEN ACCESS

Article

Lessons learned from pre-clinical testing of xenogeneic decellularized esophagi in a rabbit model

Edward Hannon,[1,2,14] Marco Pellegrini,[1,14] Federico Scottoni,[1,3] Natalie Durkin,[1] Soichi Shibuya,[1] Roberto Lutman,[1] Toby J. Proctor,[4] J. Ciaran Hutchinson,[1,5] Owen J. Arthurs,[1,6] Demetra-Ellie Phylactopoulos,[1,7] Elizabeth F. Maughan,[1,8] Colin R. Butler,[1,9] Simon Eaton,[1] Mark W. Lowdell,[4] Paola Bonfanti,[1,7,10] Luca Urbani,[11,12] and Paolo De Coppi[1,13,15,*]

SUMMARY

Decellularization of esophagi from several species for tissue engineering is well described, but successful implantation in animal models of esophageal replacement has been challenging. The purpose of this study was to assess feasibility and applicability of esophageal replacement using decellularized porcine esophageal scaffolds in a new pre-clinical model. Following surgical replacement in rabbits with a vascularizing muscle flap, we observed successful anastomoses of decellularized scaffolds, cues of early neovascularization, and prevention of luminal collapse by the use of biodegradable stents. However, despite the success of the surgical procedure, the long-term survival was limited by the fragility of the animal model. Our results indicate that transplantation of a decellularized porcine scaffold is possible and vascular flaps may be useful to provide a vascular supply, but long-term outcomes require further pre-clinical testing in a different large animal model.

INTRODUCTION

Esophageal replacement is the primary surgical option in many cases of severe congenital malformations such as long-gap esophageal atresia (OA), failure of initial OA surgery, or acquired esophageal pathologies including full thickness injury due to ingestion of caustic substances or esophageal cancer (Maghsoudlou et al., 2014). In these circumstances, a large tissue deficit means primary anastomosis may not be feasible. Current techniques for esophageal substitution include using the stomach, large intestine or more rarely, the small intestine; however, these options have significant associated mortality and morbidity including prolonged hospital stays, anastomotic stricture, and chronic reflux with increased risks of cancer; alternative solutions are therefore warranted.

Tissue engineering offers a possible solution to repair tubular defects via the use of synthetic or natural scaffolds (Boys et al., 2020; Catry et al., 2017; Cesur et al., 2021; Luc et al., 2018; Poghosyan et al., 2015; Takeoka et al., 2019; Williams, 2019). We recently proposed a tissue-engineered solution by combining a decellularized esophagus with mesenchymal and epithelial cells (Urbani et al., 2018). Rat esophageal scaffolds were decellularized and the muscularis repopulated with myogenic cells (human mesoangioblasts), murine fibroblasts, and neural crest cells. After *in vitro* maturation, the graft was successfully vascularized *in vivo* upon omental implantation. Having achieved this in a small animal model in a heterotopic position, we wanted to develop a larger animal model to assess orthotopic transplantation of tissue-engineered porcine esophageal scaffolds as a pre-clinical testing model.

Several large animal models have been described for implantation of tissue-engineered esophagi including dogs (Badylak et al., 2005), pigs (Poghosyan et al., 2015), and rabbits (Saito et al., 2000). The selection of an animal model must consider scale and size compared to the planned clinical application, anatomical and physiological similarity to humans, robustness of animals, costs, animal legislation, and ethical issues. Dogs were used in one of the earliest models for esophageal implantation and appear to have been a robust model with good results in terms of survival—up to 45 days following circumferential implantation (Badylak et al., 2000, 2005). However, their

[1]Great Ormond Street Institute of Child Health, University College London, London WC1N 1EH, UK

[2]Department of Paediatric Surgery, Leeds Children's Hospital, Leeds Teaching Hospitals NHS Trust, Leeds LS1 3EX, UK

[3]Department of Pediatric Surgery, Regina Margherita Children's Hospital, Turin 10126, Italy

[4]Centre for Cell, Gene and Tissue Therapies, Royal Free Hospital & University College London, London NW3 2PF, UK

[5]Department of Histopathology, Great Ormond Street Hospital for Children NHS Foundation Trust, London WC1N 3JH, UK

[6]Department of Radiology, Great Ormond Street Hospital for Children NHS Foundation Trust, London WC1N 3JH, UK

[7]Epithelial Stem Cell Biology & Regenerative Medicine Laboratory, The Francis Crick Institute, London NW1 1AT, UK

[8]Charing Cross Airway Service, Department of Otolaryngology, Charing Cross Hospital, Imperial Healthcare NHS Trust, London W6 8RF, UK

[9]ENT Department, Great Ormond Street Hospital for Children NHS Foundation Trust, London WC1N 3JH, UK

[10]Institute of Immunity & Transplantation, University College London, London NW3 2PP, UK

[11]The Roger Williams Institute of Hepatology, Foundation for Liver

Continued

This is an open access article under the CC BY-NC-ND license (http://creativecommons.org/licenses/by-nc-nd/4.0/).

availability, cost, and ethical barriers strongly limit the use of dogs for pre-clinical studies. More recently, porcine models have been the most commonly used large animal model. In particular, for esophageal replacement, pigs have the advantage of a long cervical esophagus allowing for implantation in the neck rather than requiring a thoracotomy. Recent studies have demonstrated the robustness of the porcine model following circumferential cervical and intra-abdominal implantation of acellular scaffolds alongside omental vascularization (Poghosyan et al., 2015; Catry et al., 2017; Levenson et al., 2021). Pigs, however, remain very expensive in terms of housing and post-operative care, and as such their use is often restricted to the later stages (*i.e.*, immediately pre-clinical) of a translational program as they remain classified as a large animal. As one of the clinical challenges of the translational program of work is to produce a tissue-engineered esophagus for implantation in infants with esophageal atresia at around 3 months of age, we evaluated the use of an animal model with an adult weight comparable to a human infant of that age. New Zealand white rabbits are suitable, as they have a long neck allowing relatively easy access to the cervical trachea and esophagus, they weigh approximately 3.5 kg at 20 weeks of age, and they have previously been used to model long-gap esophageal atresia surgical repair (Glenn et al., 2017).

The aim of this study was to develop a new animal model of esophageal replacement to be used for pre-clinical testing of tissue-engineered esophageal substitutes for the treatment of pediatric OA. To be clinically translatable in pediatric patients, this surgical model was designed using parameters that reflected the pediatric esophagus diameter and length, with replacement organs provided by decellularized porcine esophageal scaffolds.

RESULTS

The use of a decellularization chamber and the DET protocol results in successful decellularization of piglet esophagi

Portions or whole-length porcine esophagi were placed inside a custom decellularization chamber (Figure 1A). After three cycles of detergent enzymatic treatment (DET) protocol, macroscopic observation revealed decellularized, pale esophagi that were comparable in size to the native tissue (Figure 1A). A complete clearance of nuclear material was demonstrated by histological examination and DNA quantification (Figures 1B and 1D). Histological examination also revealed successful preservation of the microarchitecture, with the mucosa, submucosa, and muscularis externa still clearly identifiable (Figure 1B). Fibril-forming collagen type I was ubiquitously distributed throughout the extracellular matrix (ECM) pre- and post-decellularization, and fibronectin, collagen type IV, and laminin immunofluorescence staining revealed intact basement membranes were also preserved following decellularization (Figure 1C). Collagen retention was also confirmed by a significant increase in normalized total concentration (Figure 1D). Conversely, quantification of normalized sulfated glycosaminoglycan (sGAG) content in the decellularized esophagi revealed a non-significant decrease in concentration as has been previously reported after esophageal decellularization (Totonelli et al., 2013; Urbani et al., 2017) (Figure 1D).

Measurement of the biomechanical properties of native and decellularized specimens was performed to understand the similarity between the two. Longitudinally orientated specimens were used as a reflection of the physiological strain that esophagi experience *in vivo* during swallowing. Of note, in humans, the muscularis externa of the proximal esophagus is predominantly striated muscle, while the distal part transitions to smooth muscle. This composition is also reflected in the porcine esophagus (La Francesca et al., 2018). For this reason, the stiffness, ultimate stress, and ultimate strain of tissue biopsied from the upper and lower thirds of the organ were evaluated pre- and post-decellularization. No significant differences in the biomechanical profiles were observed between native and decellularized esophageal segments (Figure 1E). Finally, the suitability of the scaffold as a conduit for food and liquid was assessed by a fluid bolus test with methylene blue; no leakage of dye after 10 min indicates excellent integrity of the acellular scaffold wall and clinical suitability as an esophageal conduit (Video S1).

Surgical protocol design

Implantations of the scaffolds were performed in three phases based on systematic surgical protocol adaptations (Figure 2 and graphical abstract):

Phase One – A pilot study was designed to assess the feasibility of esophageal replacement in the rabbit surgical model. The scaffold was orthotopically anastomosed in a single-stage surgery.

Phase Two – A two-stage approach was used. At stage one, a biodegradable stent was applied in the decellularized scaffold's lumen and implanted in a muscle flap in the rabbit's neck for two weeks of pre-vascularization. At the second stage, the vascularized graft was orthotopically anastomosed into the cervical esophagus and a gastrostomy performed to allow for better animal feeding.

Research, London SE5 9NT, UK

[12]Faculty of Life Sciences and Medicine, King's College London, London SE5 8AF, UK

[13]Specialist Neonatal and Paediatric Surgery, Great Ormond Street Hospital for Children NHS Foundation Trust, London WC1N 3JH, UK

[14]These authors contributed equally

[15]Lead contact

*Correspondence: p.decoppi@ucl.ac.uk

https://doi.org/10.1016/j.isci.2022.105174

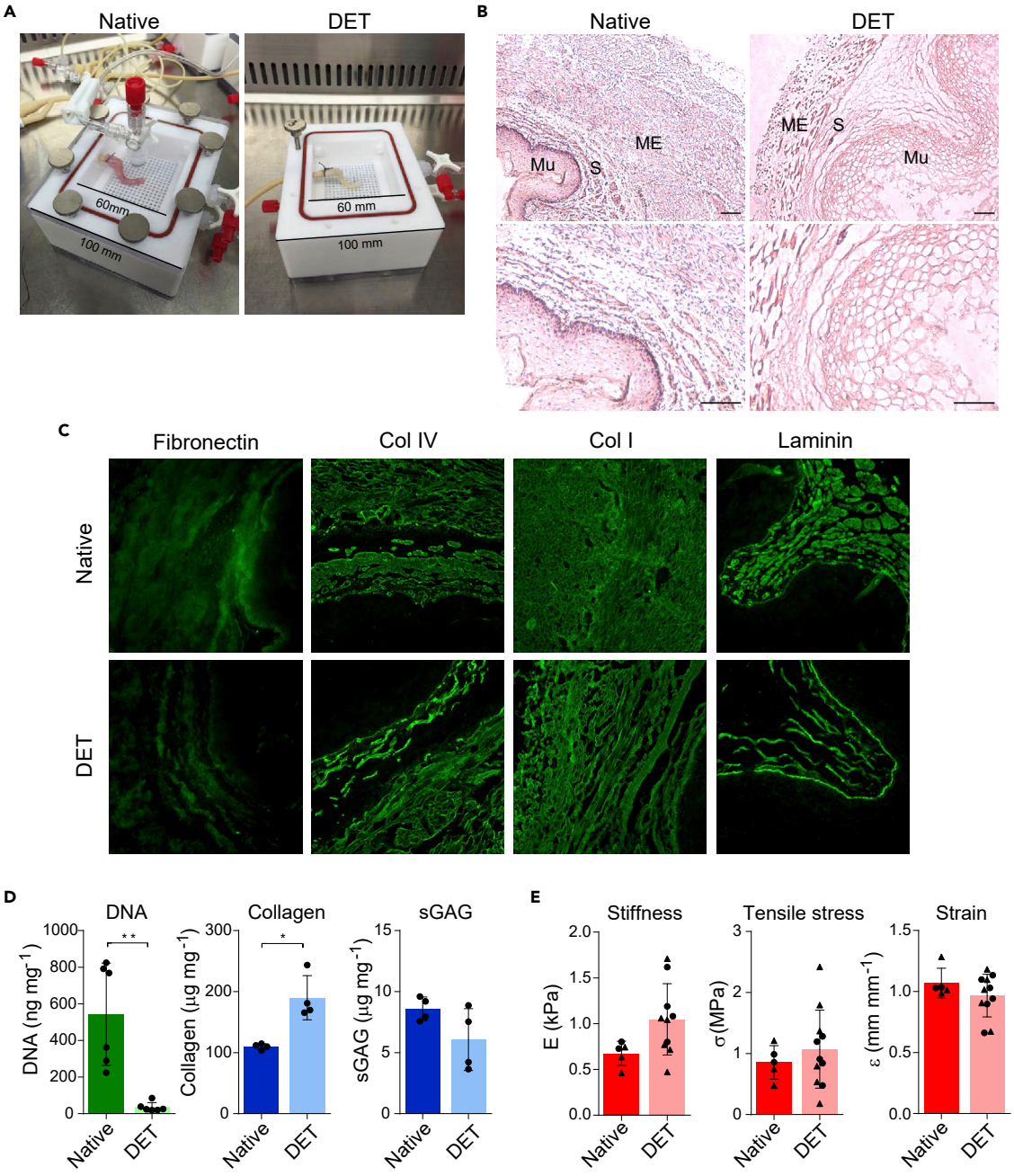


Figure 1. Piglet esophagus decellularization with DET protocol and ECM characterization

(A) The esophagi were decellularized in custom chambers. Here a representative esophagus before (native, left) and after (DET, right) the decellularization process is shown.

(B) Hematoxylin and eosin (H&E) staining of native (left) and DET tissue (right). ME: muscularis externa. S: submucosa. Mu: mucosa. Scale bar: 100 µm.

(C) Immunofluorescence staining for Fibronectin, Collagen IV, Collagen I, and Laminin in native and DET tissue. Scale bar: 50 µm. Both H&E and immunofluorescence show a good preservation of the ECM.

(D) DNA quantification shows a significant reduction of DNA following three cycles of DET ($p < 0.01$, $n = 6$). Total collagen ($p < 0.05$, $n = 4$) and sGAG ($n = 4$) content were preserved. Bars indicate mean ± SD, circles represent biological replicates.

(E) Biomechanical analysis of native and decellularized samples derived from proximal (circle) or distal (triangle) portions of the esophagi. Stiffness (native $n = 5$; DET $n = 10$), ultimate tensile stress (native $n = 5$; DET $n = 11$), and ultimate strain (native $n = 5$; DET $n = 11$) were evaluated. Bars indicate mean ± SD, circles and triangles represent biological replicates of tissue biopsied from the upper and lower thirds of the organ, respectively.

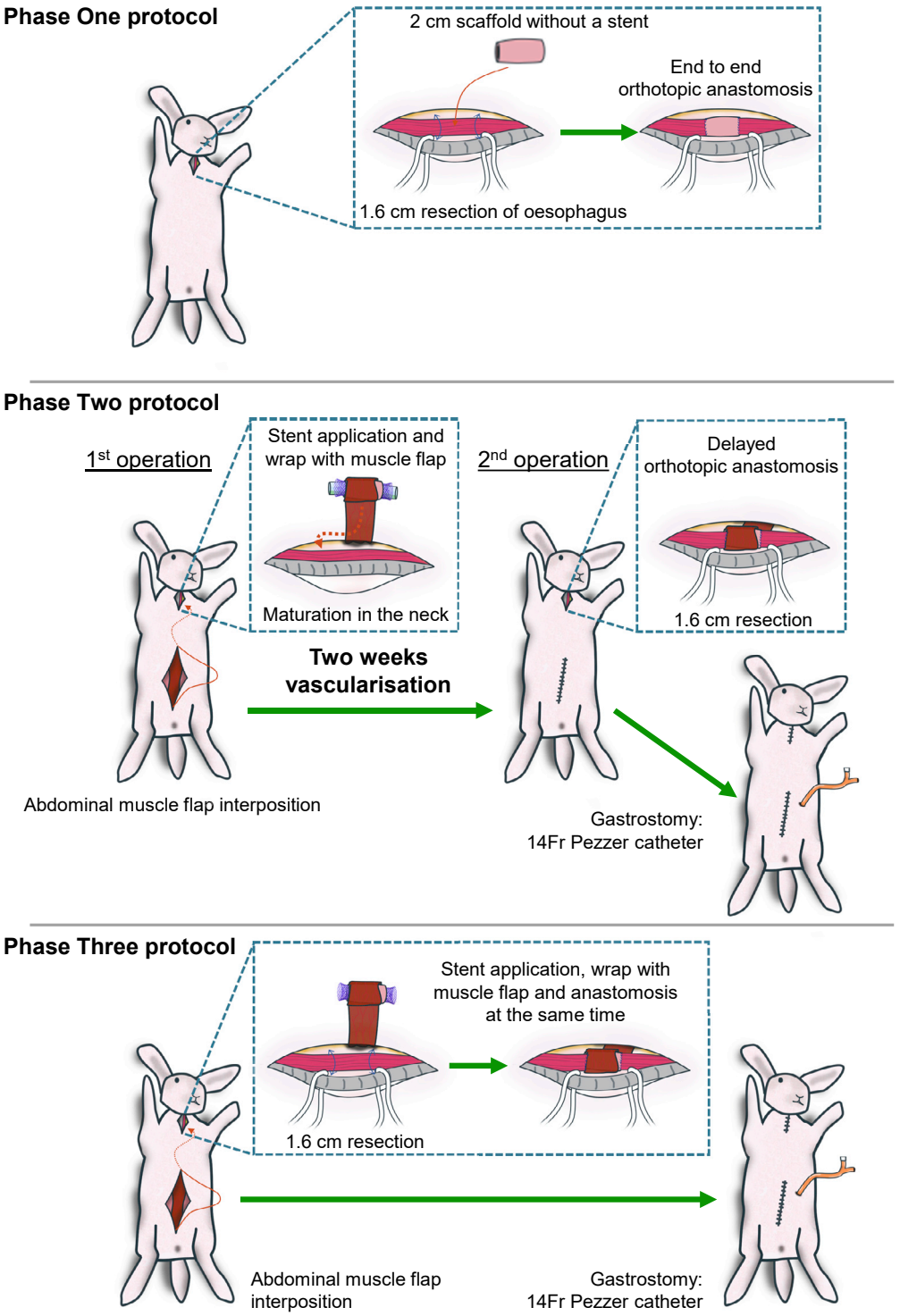


Figure 2. Summary of the three surgery protocols applied in the study

Phase One: orthotopic anastomosis of decellularized scaffold. Phase Two: pre-implantation of scaffold in the neck in vascularizing muscle wrap with application of intra-luminal stent followed by orthotopic cervical anastomosis two weeks later. Phase Three: a single-stage anastomosis was performed with a muscle wrap and stent and concomitant gastrostomy formation.

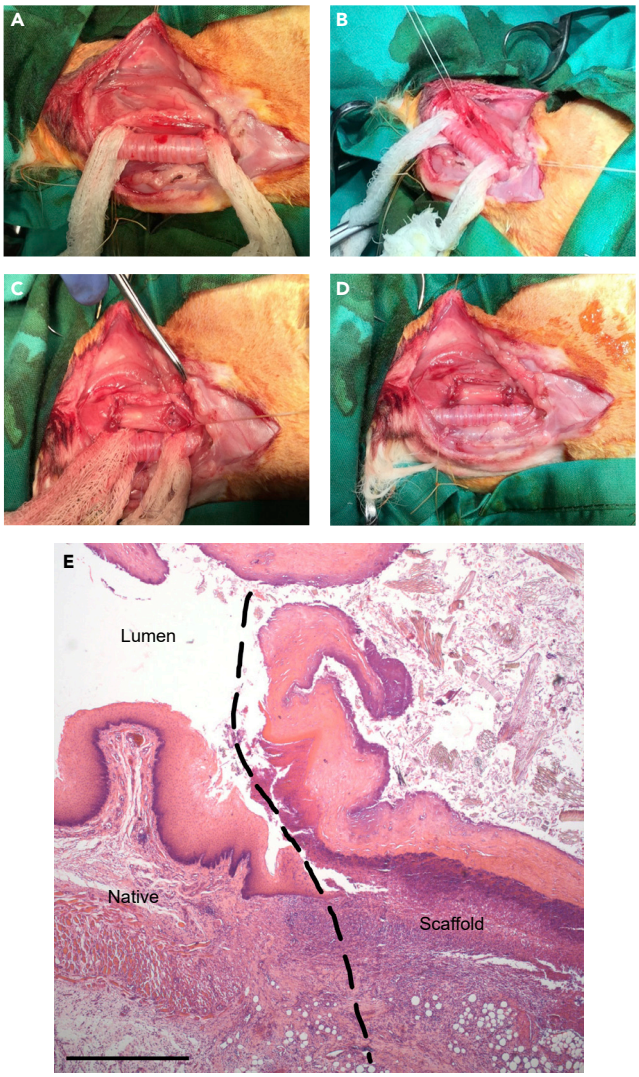


Figure 3. Operative stages of Phase One: esophageal scaffold implantation

(A) Trachea exposure.

(B) Rabbit esophagus resection.

(C) Porcine esophageal scaffold positioning.

(D) Orthotopic anastomosis of the scaffold.

(E) H&E staining of porcine scaffold following implantation in cervical rabbit esophagus; longitudinal section at the anastomosis level (dashed line) from an animal euthanized at post-operative day nine. Scale bar 250 μm.

Phase Three – Due to the fragility of rabbits and their limited survival during a two-stage approach, a single-stage surgery was performed with adaptations from Phase Two. During the operation, the stented esophageal scaffold was directly wrapped in a vascularizing muscle flap and orthotopically anastomosed into the cervical esophagus with concomitant gastrostomy formation.

Direct orthotopic anastomosis of esophageal scaffolds (Phase One) does not allow for long-term survival

In Phase One, rabbits were positioned prone and fur shaved. A longitudinal incision was made in the neck and the strap muscles spread laterally (see Methods for details). The trachea was exposed and dissected ensuring preservation of the recurrent laryngeal nerves (Figure 3A). The cervical esophagus was then mobilized (Figure 3B) and a 1.6 cm circumferential segment of native esophagus was resected. A similar sized circumferential segment of

Table 1. Results of surgeries from Phase One (n = 6)

Conditions	Survival (days)	Reasons for euthanasia
Primary anastomosis	0; 0	Anesthetic (n = 2)
	3; 9	Respiratory distress (n = 2)
	7	Weight loss (n = 1)
	9	Fur obstruction (n = 1)

decellularized porcine scaffold was then (Figure 3C) anastomosed to the native esophagus with monofilament sutures (Figure 3D) and the wound was closed and infiltrated with lignocaine.

Early in Phase One, two animals were euthanized due to anesthetic problems; a laryngeal mask airway (v-gel®) was added in order to allow hand ventilation to rabbits in case of respiratory distress during the procedure—especially during mobilization of the trachea. This change led to a decrease in anesthetic problems in later phases of the study.

Two animals were euthanized 3 and 9 days post surgery due to respiratory distress. It was not possible to determine the specific cause, but appeared to be the result of recurrent laryngeal nerve damage or aspiration due to early collapse and obstruction of the unsupported scaffold (Table 1).

In all animals surviving surgery, post-operative feeding was a problem. Most animals were disinterested in feeding orally, and in those attempting to eat, it was apparent that there were difficulties in swallowing. In one animal that survived to seven days postoperatively, poor oral intake resulted in weight loss (>10% body weight), which was the reason for euthanasia, in line with the humane endpoint specified in the project license. In another case, obstruction of the scaffold with fur was the reason for euthanasia (Table 1). Following this pilot study, a number of modifications were implemented in Phase Two to address the problems encountered.

Despite poor animal survival, histological analysis of scaffold collected 9 days post implantation showed a good integration with native tissue at the anastomosis level (Figure 3E).

The use of a muscle flap improves scaffold vascularization but the two-stage protocol for orthotopic scaffold anastomosis (Phase Two) impairs animal survival

In order to maximize maturation of the scaffold, a two-stage model was proposed and trialed in animals. This had been successful in rat esophagus tissue engineering (Urbani et al., 2018) and the approach was therefore adapted for the porcine esophageal scaffold implantation in rabbits.

Various modifications were made to the operative technique in order to maximize survival outcomes. These included: *1) Gastrostomy feeding*: Stamm-type gastrostomies were used to ameliorate post-operative feeding problems and mirror what would happen in clinical practice in babies with long-gap OA (Figure 4A). A 14Fr Pezzer catheter was chosen based on experience with its use clinically, with the advantage of a wide bore to allow for delivery of a high-fiber, viscous diet via the tube. In order to minimize obstruction of esophageal scaffolds, a veterinarian type collar was applied to animals alongside the gastrostomy to reduce grooming and to coprophagia practices. *2) Esophageal luminal stent*: due to the known risk of longer term strictures observed in other engineered esophageal models, and the episode of esophageal obstruction in Phase One, stenting of the scaffold was introduced. Biodegradable BD stents were selected based on previous clinical experience and their mechanical properties; they have enough rigidity to maintain scaffold patency balanced with sufficient elasticity to avoid excess pressure on the graft and healing anastomoses. Scaffolds were pre-mounted onto the stent before graft implantation (Figure 4B). *3) Vascularizing muscle flap*: vascularization of any tissue-engineered organ is advantageous as it has been shown to promote infiltrating cell survival, engraftment, and eventually graft function (Elliott et al., 2012; Pellegata et al., 2018). However, the segmental vascular anatomy of the esophagus makes this an additional challenge. We introduced the use of anterior abdominal wall muscle flaps based on branches of the superior epigastric vessels, a technique previously successfully used to vascularize engineered tracheal grafts (Maughan et al., 2017) (Figures 4C–4E).

Table 2. Results of surgeries from Phase Two (n = 7)

Conditions	Survival (days post anastomosis)	Reasons for euthanasia
Primary insertion of stented scaffold in vascularizing flap	0; 0	Anesthetic (n = 2)
Delayed anastomosis	0; 2	Scaffold remodeling (n = 2)
Gastrostomy	4; 7	Fur obstruction (n = 2)
	6	Mortality following flap infection (n = 1)

The two-stage model involved initial implantation of the decellularized scaffold in the muscular vascularizing flap which was left in the neck to allow neovascularization of the scaffold. After two weeks, at the second stage of surgery, a 1.6 cm long section of the native esophagus was resected and the wrapped scaffold was orthotopically anastomosed; finally, a gastrostomy was inserted. Both the gastrostomy and surgery were well tolerated; however, multiple problems with gastrostomy tubes were experienced in the post-operative period. The main problem was tube obstruction caused by the position on the animal, the soft silicone nature of the tubing, and high fiber content of the diet provided. Although the soft tube was well tolerated as it was comfortable for the animal, efforts to unblock it damaged the tube and on one occasion resulted in displacement.

Two rabbits were lost due to anesthetic complications during Phase Two, and in further two animals, a prolonged anesthetic due to difficulties in surgical handling of the scaffold due to remodeling after pre-vascularization likely resulted in their demise on day 0 and 2, respectively (Table 2). Three animals that survived both stages had scaffold and muscle wraps that appeared macroscopically well vascularized (Figure 4F) and this offered the benefit of improved suture retention during anastomosis (Figure 4G). However, overgranulation was observed in the lumen of the scaffold despite the presence of the intra-luminal stent between the two stages (Figure 5A) and subsequent survival in these animals was again limited by obstruction. Histology confirmed the presence of microvascularization within the muscularis layer and luminal overgranulation (Figure 5B). The overall post-operative survival was reduced following the two-stage procedure compared to the Phase One of study (Figure 5C).

A single-stage approach (Phase Three) that combines gastrostomy, luminal stent, and vascularizing flap increases animal survival upon scaffold anastomosis

Since a two-stage approach was strongly limited by the fragility of the rabbit model, we modified the surgical approach further by using a single-stage surgery combining all the procedures introduced in Phase Two concomitantly with the orthotopic anastomosis. The vascularizing wrap was well tolerated despite the need for a long additional incision in the abdomen. The graft was relatively uncomplicated to mobilize but given it was very thin and on the narrow vascular pedicle of the muscle, three animals suffered from necrosis of the flap leading to collections around the scaffold.

Animals with uncomplicated recovery from surgery tended to present with bolus obstruction which limited their survival (Figure 6A), a recurring problem throughout the study despite the addition of gastrostomy feeding. In these animals, survival ranged from 2 to 15 days with a median survival of 6 days (Table 3, fur obstruction). In one of these animals, bolus obstruction was noted at day 5, with successful endoscopy and removal of a fur bolus. The animal survived until day 10 when it was euthanized because of respiratory distress.

Stenting appeared to be beneficial in the early post-operative period, as it prevented early collapse of the scaffold however may have contributed to fur bolus obstruction due to its woven structure and the relative decrease in luminal diameter due to its presence. Histological and immunofluorescence analyses showed evidence of good integration and the beginning of cell infiltration in the scaffold (Figure 6B) even after only four days post-surgery (Figure S1). Examination using iodine-enhanced micro-CT permitted postmortem observation of the stent *in situ* before dissecting the scaffold. This demonstrated appropriate positioning of the stent within the scaffold, with luminal patency throughout the entire length of the specimen, and a close approximation between the stent and the underlying scaffold submucosa. The anastomotic sites also appeared viable, intact, and well approximated, with no features of tissue necrosis. (Figure 6C; Video S2).

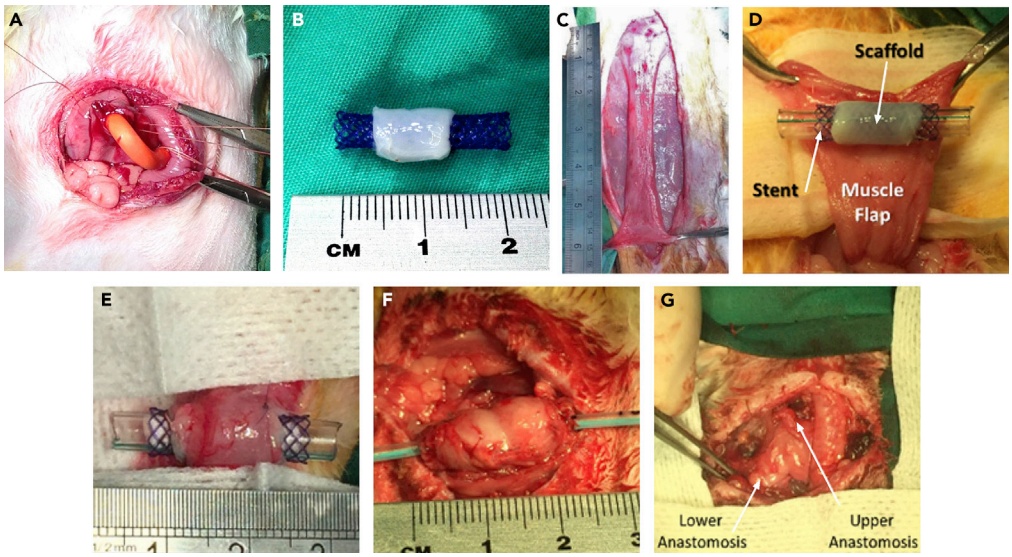


Figure 4. Surgical improvements applied from Phase Two

(A) Tunneled Stamm gastrostomy formation using a 14Fr Pezzer catheter.

(B) Scaffold pre-mounted on stent.

(C) An anterior abdominal wall flap was prepared, (D) tunneled to neck and (E) sutured around the scaffold.

(F) After two weeks, at the second surgical stage, the vascularized graft was mobilized and (G) anastomosed in orthotopic position.

Overall survival was best in Phase Three using the combination of the single-stage approach with gastrostomy feeding, luminal stenting, and the muscle flap (Figure 5C).

DISCUSSION

Whole organ tissue engineering may offer a solution for a variety of conditions where organ replacement is required. Encouraging clinical results have been obtained from tissue-engineered tracheal replacements (Elliott et al., 2012), but such translation from the lab to the patient is yet to be possible for full-thickness circumferential esophageal replacements.

Our results demonstrate that esophageal replacement with a circumferential decellularized porcine scaffold is feasible in a rabbit model but has several limitations, which precludes its use for further clinical studies in humans. The innovative process of model design and modifications led to an improved understanding of some of the challenges the transplant of tissue-engineered esophagus may bring in different large animal models and eventually in the clinical setting and more importantly how these challenges can be overcome.

Scaffold selection for tissue engineering is the first step in designing a tissue-engineered esophageal replacement and it is still a much-debated subject (Jensen et al., 2015; Poghosyan et al., 2015; Park et al., 2016; Catry et al., 2017; Lee et al., 2017; La Francesca et al., 2018; Levenson et al., 2021). Our group favors a decellularized xenogeneic scaffold, and has demonstrated the benefits of this approach *in vitro* including excellent maintenance of ECM structure and the resulting improvement in engraftment of seeded stem cells (Urbani et al., 2018). This is true in various organ ECMs where maintaining an intact matrix structure is associated with beneficial functional outcomes. For example, decellularized liver matrices help functional hepatic differentiation of pluripotent stem cells (Lorvellec et al., 2020), and decellularized intestinal matrices help functional differentiation of human small intestinal organoids after expansion (Meran et al., 2020). The *in vivo* results obtained also demonstrated that in addition to providing an excellent stem cell niche, the properties of decellularized porcine esophageal scaffolds may make them suitable for successful implantation in larger animals. Confirmation findings from the mechanical tests performed on the decellularized tissue which highlighted good preservation of mechanical features, scaffolds handled well during implantation, and demonstrated excellent suture retention. No animals in the Phase Three

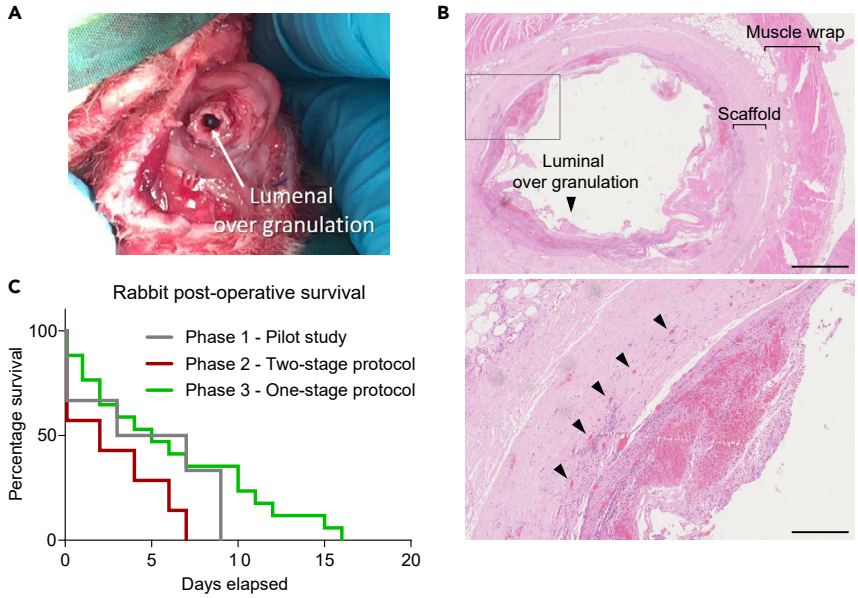


Figure 5. Second stage of Phase Two procedure and analysis of post-operative survival

(A) Macroscopic overgranulation within the lumen of the scaffold.

(B) H&E staining of scaffold seven days post second stage orthotopic implantation, sliced transversely across lumen, showing cues of both luminal granulation (arrowhead in top panel) and microvascularization (arrowheads in bottom panel). Top panel scale bar 2.5 mm; bottom panel scale bar 500 μm.

(C) Kaplan-Meier survival curve by study groups of Phase One (pilot study, n = 6), Phase Two (two-stage protocol, n = 7) and Phase Three (single-stage protocol, n = 15).

group were lost due to scaffold failure or rupture, supporting the use of decellularized scaffolds when suitable surgical modifications are applied such as stent usage and vascularizing flaps.

Maintenance of the lumen of tubular esophageal scaffolds is the most frequently reported complication limiting the long-term outcome of *in vivo* models (Doede et al., 2009; Gaujoux et al., 2010; Poghosyan et al., 2015). This problem led to the use of biodegradable stents at implantation. Gaujoux and colleagues used non-absorbable polyester covered stents in a pig model, implanting allogenic aorta as the esophageal graft and reported several complications from stent migration (Gaujoux et al., 2010). Biodegradable PDS stents, which we have clinical experience using after tissue-engineered tracheal implantation, were therefore used. Pre-mounting the scaffold onto the stent and securing it in place resulted in no early scaffold migration. The benefit of an uncovered stent is that over time it becomes integrated avoiding migration, but this must be balanced with the risk of granulation tissue overgrowing the stent into the lumen over longer term, as was seen in the two-stage model. Appropriate stent position without migration is well demonstrated in the micro-CT images. The lumen is patent throughout the length of the specimen. The anastomotic sites, *submucosa* and *muscularis propria* show appropriate tissue organization, including orientation of smooth muscle fibers. An abnormal connection with the trachea (*e.g.*, a fistula) can also be excluded from analysis of the micro-CT volume (Figure 5C). Stent usage prevented the early collapse of the scaffold maintaining luminal patency. Scaffold obstruction in those animals surviving to later time points was predominantly as a result of the coprophagic and fur ingestion behavior typical of rabbits, which adhered to the stent resulting in obstruction. This is an obvious limitation of the model, and may still occur regardless of anatomical location of orthotopic transplantation (*e.g.*, intra-thoracic or intra-abdominal). An alternative option to consider may be external stenting of the esophagus with biodegradable stents as previously trialed in tracheal reconstruction in rabbits with some success compared to controls (Robey et al., 2000). However, a more comprehensive option would be to use an animal model which does not practice coprophagy or have fur as is the case in porcine models and is more reflective of clinical practice.

Vascularization of whole tissue-engineered organs remains a challenge, especially with the segmental blood supply of the native esophagus which limits a pre-vascularization *in vitro* approach which has been adopted for other organs such as intestine or lung (Meran et al., 2020; Ren et al., 2015). Various

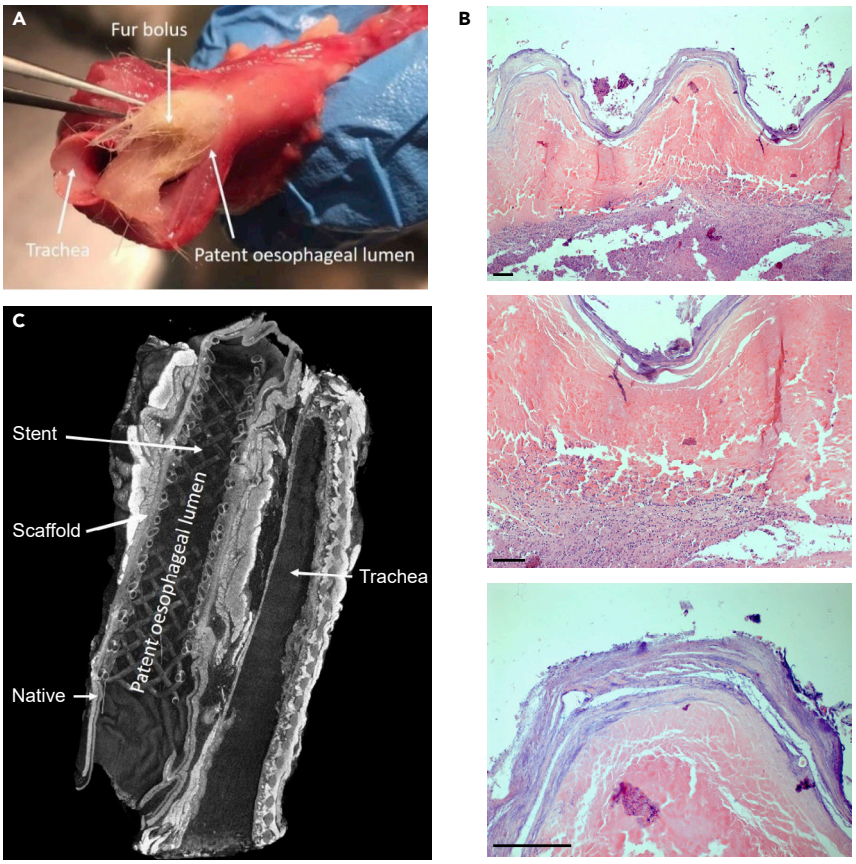


Figure 6. Results of surgery from Phase Three

(A) Fur bolus obstruction in autopsy specimens from an animal euthanized at day 15.

(B) H&E of porcine scaffolds following single-stage orthotopic anastomosis in cervical rabbit esophagus with vascularizing flap, collected from an animal euthanized at day 16; Top panel 5× magnification, middle panel 10× magnification, bottom panel 20× magnification. Scale bar 50 μm.

(C) Micro-CT of *en bloc* resection of esophagus and trachea after 10 days *in vivo* demonstrating excellent luminal patency and anastomosis to native esophagus. See also Figure S1 and Video S2.

strategies have been suggested including the use of vascularizing pedicles or flaps and the use of angiogenic factors such as VEGF applied to scaffolds (Chung et al., 2018; Hamaji et al., 2014; Urbani et al., 2018). We chose to use an anterior abdominal wall muscle flap—as has previous been described for tracheal (Delaere et al., 1995; Den Hondt et al., 2016) and esophageal (Saito et al., 2000) scaffold vascularization. This vascularizing muscle flap is easily harvested from the rabbit anterior abdominal wall and avoids the morbidity of thoracotomy (which would be poorly tolerated in rabbits) to deliver an omental flap. The flap also provides mechanical support to the implanted scaffold and both anastomoses. Our single-stage implantation showed little neovascularization on histological examination, presumably as a result of limited survival time, usually due to luminal obstruction or gastrostomy failure. The two-stage model with prevascularization in the muscle flap before orthotopic implantation at a second stage demonstrated evidence of neovascularization after 2 weeks *in vivo* macroscopically, which was confirmed by histological examination. Larger, more robust models have used transthoracic omental flaps successfully (Poghosyan et al., 2015) and in clinical practice this may be a more useful approach given that anastomoses would need to be intra-thoracic rather than cervical. Additionally, clinical experience using this technique already exists from tracheal replacement (Elliott et al., 2012).

The main issue related to the gastrostomy tubes was obstruction. We believe this was the result of a combination of factors including: i) nutrition—rabbits require a high-fiber diet for gut health. However, even the "fine grind" feed used in all three stages of our protocol was too viscous and tended to block the malecot tube; ii) tube choice—the 14Fr silicone tube was selected as it is soft and as such would be easily tunneled

Table 3. Results of surgeries from Phase Three (n = 15)

Conditions	Survival (days)	Reasons for euthanasia
Primary anastomosis	0; 0	Anesthetic (n = 2)
Esophageal stent	1	Scaffold remodeling (n = 1)
Gastrostomy	2; 2; 10; 15	Fur obstruction (n = 4)
Vascularizing wrap	4; 5; 6; 7; 12	Gastrostomy failure (n = 5)
	10; 11; 16	Flap infection/necrosis (n = 3)

subcutaneously and not cause pressure ulcers at its exit site, resulting in a high tolerability from the animal. Unfortunately, however, the softness of the tube made it very difficult to unblock when obstructed and tube dislodgement was also a problem during attempts to unblock them.

This study of esophageal tissue engineering, animal model development, and modification has added useful and encouraging data to the existing literature and experience. It has demonstrated that the rabbit model while useful in early experimental development is not robust enough to move forward with pre-clinical work. Its usefulness as a comparable size to the neonatal patient is limited by its fragility as a surgical model and in the longer term by the unavoidable ingestion of fur and feces leading to luminal obstruction as seen in a similar Japanese study (Saito et al., 2000). Indeed, there are surgical limitations to the model which affect a definitive pre-clinical outcome. Rabbits are a prey animal making them prone to being less robust than porcine or dog models. They also have specific dietary requirements (Thomas et al., 2012), requiring large amounts of fiber in their food to prevent gastrointestinal upset and potentially fatal colitis. They also routinely practice coprophagy and often groom vigorously which is important to consider when planning to replace segments of the proximal esophagus.

The suitability of decellularized porcine scaffolds for esophageal implantation with no emergence of immunogenic effects was confirmed, but the need for early scaffold support with absorbable stenting is recognized. It appears that vascularizing flaps will play a role in the future development of further pre-clinical models, but a single-stage approach is preferable in fragile models with porcine models being the most favorable next stage of development. The larger size of even the mini-pig (10–25kg) makes the clinical comparison to neonatal patients compatible with pediatric intervention. Moreover, the benefit of a more robust animal model (Gaujoux et al., 2010; Poghosyan et al., 2015) should result in longer survival and allow implantation of recellularized scaffolds.

Limitations of the study

While a rabbit model for *in vivo* implantation of tissue-engineered esophagi is feasible, it is not robust enough to allow long-term survival with outcomes limited by obstruction of the scaffold and respiratory complications despite the use of intra-luminal stents. A more robust and reproducible large animal model is required prior defining a product suitable to clinical translation.

STAR★METHODS

Detailed methods are provided in the online version of this paper and include the following:

- KEY RESOURCES TABLE
- RESOURCE AVAILABILITY
  - Lead contact
  - Materials availability
  - Data and code availability
- EXPERIMENTAL MODEL AND SUBJECT DETAILS
  - Surgical protocol
- METHOD DETAILS
  - Organ collection and scaffold preparation
  - Histological analysis
  - Immunofluorescence
  - DNA quantification
  - ECM component quantification

- Biomechanical tests
- Fluid bolus test
- Micro-CT scan

- QUANTIFICATION AND STATISTICAL ANALYSIS

SUPPLEMENTAL INFORMATION

Supplemental information can be found online at https://doi.org/10.1016/j.isci.2022.105174.

ACKNOWLEDGMENTS

P.D.C. is supported by National Institute for Health Research (NIHR-RP-2014-04-046). L.U. was supported by NIHR and the Oak Foundation (W1095/OCAY-14-191). S.E. and N.D. are supported by Great Ormond Street Hospital (GOSH) Children's Charity. P.B. is supported by the UCL Excellence Fellowship Program, the Rosetrees Trust (M362; M362-F1; M553) and the NIHR Biomedical Research Center at Great Ormond Street Hospital for Children NHS Foundation Trust. M.P. is supported by the Horizon 2020 grant INTENS 668294. This study was supported by the UK Stem Cell Foundation, the Cell and Gene Therapy Catapult, the GOSH Charity (V1282), and the Oak Foundation. NIHR support was dedicated exclusively to the human cells used in the paper. All research at Great Ormond Street Hospital NHS Foundation Trust and UCL Great Ormond Street Institute of Child Health is made possible by the NIHR Great Ormond Street Hospital Biomedical Research Center. The views expressed are those of the author (s) and not necessarily those of the NHS, the NIHR, or the Department of Health. The graphical abstract was created with "BioRender.com". The authors would like to thank Martin Birchall, Carlotta Camilli, and Claire Crowley for the discussion, technical help, and support.

AUTHOR CONTRIBUTIONS

E.H., L.U., M.W.L., P.B., P.D.C designed the work. E.H., M.P., F.S., T.J.P., J.C.H., N.D., R.L., O.J.A., D.E.P., E.F.M., C.R.B., S.E., M.W.L., P.B., L.U., P.D.C. performed the experiments and contributed to data collection. E.H., M.P., F.S., T.J.P., J.C.H., O.J.A., D.E.P., E.F.M., C.R.B., S.E., M.W.L., P.B., L.U., P.D.C. contributed to data analysis and interpretation. E.H., M.P., T.J.P., S.S., J.C.H., M.W.L., P.B., L.U., P.D.C. prepared the figures. E.H., M.P., L.U., P.D.C. wrote the manuscript. E.H., M.P., F.S., N.D., R.L., S.S., T.J.P., J.C.H., O.J.A., D.E.P., E.F.M., C.R.B., S.E., M.W.L., P.B., L.U., P.D.C. contributed to the revision of the manuscript.

DECLARATION OF INTERESTS

P.D.C. and L.U. are named inventors of patent application No. PCT/EP2016/071114 and P.D.C. and L.U. are named inventors of UK patent application No. 1708729.7. The remaining authors declare no competing interests.

Received: December 13, 2021
Revised: June 21, 2022
Accepted: September 19, 2022
Published: October 21, 2022

REFERENCES

Badylak, S.F., Vorp, D.A., Spievack, A.R., Simmons-Byrd, A., Hanke, J., Freytes, D.O., Thapa, A., Gilbert, T.W., and Nieponice, A. (2005). Esophageal reconstruction with ECM and muscle tissue in a dog model. J. Surg. Res. *128*, 87–97. https://doi.org/10.1016/j.jss.2005.03.002.

Badylak, S., Meurling, S., Chen, M., Spievack, A., and Simmons-Byrd, A. (2000). Resorbable bioscaffold for esophageal repair in a dog model. J. Pediatr. Surg. *35*, 1097–1103. https://doi.org/10.1053/jpsu.2000.7834.

Boys, A.J., Barron, S.L., Tilev, D., and Owens, R.M. (2020). Building scaffolds for tubular tissue engineering. Front. Bioeng. Biotechnol. *8*, 1–20. https://doi.org/10.3389/fbioe.2020.589960.

Catry, J., Luong-Nguyen, M., Arakelian, L., Poghosyan, T., Bruneval, P., Domet, T., Michaud, L., Sfeir, R., Gottrand, F., Cattan, P., et al. (2017). Circumferential esophageal replacement by a tissue-engineered substitute using mesenchymal stem cells. Cell Transplant. *26*, 1831–1839. https://doi.org/10.1177/0963689717741498.

Cesur, O., Tanir, T.E., Celepli, P., Ozarslan, F., Hucumenoglu, S., Karaibrahimoglu, A., and Hasirci, N. (2021). Enhancing esophageal repair with bioactive bilayer mesh containing FGF. Sci. Rep. *11*, 1–10. https://doi.org/10.1038/s41598-021-98840-w.

Chung, E.J., Ju, H.W., Yeon, Y.K., Lee, J.S., Lee, Y.J., Seo, Y.B., and Chan Hum, P. (2018). Development of an omentum-cultured oesophageal scaffold reinforced by a 3D-printed ring: feasibility of an in vivo bioreactor. Artif. Cell Nanomed. Biotechnol. *46*, 885–895. https://doi.org/10.1080/21691401.2018.1439039.

Delaere, P.R., Liu, Z.Y., Hermans, R., Sciot, R., and Feenstra, L. (1995). Experimental tracheal allograft revascularization and transplantation. J. Thorac. Cardiovasc. Surg. *110*, 728–737. https://doi.org/10.1016/S0022-5223(95)70105-2.

Den Hondt, M., Vanaudenaerde, B.M., Delaere, P., and Vranckx, J.J. (2016). Twenty years of experience with the rabbit model, a versatile model for tracheal transplantation research. Plast. Aesthet. Res. *3*, 223. https://doi.org/10.20517/2347-9264.2015.117.

Doede, T., Bondartschuk, M., Joerck, C., Schulze, E., and Goernig, M. (2009). Unsuccessful alloplastic esophageal replacement with porcine small intestinal submucosa. Artif. Organs *33*, 328–333. https://doi.org/10.1111/j.1525-1594.2009.00727.x.

Elliott, M.J., De Coppi, P., Speggiorin, S., Roebuck, D., Butler, C.R., Samuel, E., Crowley, C., McLaren, C., Fierens, A., Birchall, M.A., et al. (2012). Stem-cell-based, tissue engineered tracheal replacement in a child: a 2-year follow-up study. Lancet *380*, 994–1000. https://doi.org/10.1016/S0140-6736(12)60737-5.

Gaujoux, S., Le Balleur, Y., Bruneval, P., Larghero, J., Lecourt, S., Domet, T., Lambert, B., Zohar, S., Prat, F., and Cattan, P. (2010). Esophageal replacement by allogenic aorta in a porcine model. Surgery *148*, 39–47. https://doi.org/10.1016/j.surg.2009.12.002.

Glenn, I.C., Bruns, N.E., Gabarain, G., Craner, D.R., Schomisch, S.J., and Ponsky, T.A. (2017). Creation of an animal model for long gap pure esophageal atresia. Pediatr. Surg. Int. *33*, 197–201. https://doi.org/10.1007/s00383-016-4014-y.

Hamaji, M., Kojima, F., Koyasu, S., Tsuruyama, T., Komatsu, T., Ikuno, T., Date, H., and Nakamura, T. (2014). Development of a composite and vascularized tracheal scaffold in the omentum for in situ tissue engineering: a canine model. Interact. Cardiovasc. Thorac. Surg. *19*, 357–362. https://doi.org/10.1093/icvts/ivu177.

Jensen, T., Blanchette, A., Vadasz, S., Dave, A., Canfarotta, M., Sayej, W.N., and Finck, C. (2015). Biomimetic and synthetic esophageal tissue engineering. Biomaterials *57*, 133–141. https://doi.org/10.1016/j.biomaterials.2015.04.004.

La Francesca, S., Aho, J.M., Barron, M.R., Blanco, E.W., Soliman, S., Kalenjian, L., Hanson, A.D., Todorova, E., Marsh, M., Wigle, D.A., et al. (2018). Long-term regeneration and remodeling of the pig esophagus after circumferential resection using a retrievable synthetic scaffold carrying autologous cells. Sci. Rep. *8*, 4123. https://doi.org/10.1038/s41598-018-22401-x.

Lee, E., Milan, A., Urbani, L., De Coppi, P., and Lowdell, M.W. (2017). Decellularized material as scaffolds for tissue engineering studies in long gap esophageal atresia. Expet Opin. Biol. Ther. *17*, 573–584. https://doi.org/10.1080/14712598.2017.1308482.

Levenson, G., Berger, A., Demma, J., Perrod, G., Domet, T., Arakelian, L., Bruneval, P., Broudin, C., Jarraya, M., Poghosyan, T., et al. (2021). Circumferential esophageal replacement by a decellularized esophageal matrix in a porcine model. Surgery. https://doi.org/10.1016/j.surg.2021.07.009.

Lorvellec, M., Pellegata, A.F., Maestri, A., Turchetta, C., Alvarez Mediavilla, E., Shibuya, S., Hanson, A.D., Todorova, E., Marsh, M., Gissen, P., et al. (2020). An in vitro whole-organ liver engineering for testing of genetic therapies. iScience *23*. https://doi.org/10.1016/j.isci.2020.101808.

Luc, G., Charles, G., Gronnier, C., Cabau, M., Kalisky, C., Meulle, M., Bareille, R., Roques, S., Couraud, L., Durand, M., et al. (2018). Decellularized and matured esophageal scaffold for circumferential esophagus replacement: proof of concept in a pig model. Biomaterials *175*, 1–18. https://doi.org/10.1016/j.biomaterials.2018.05.023.

Maghsoudlou, P., Eaton, S., and De Coppi, P. (2014). Tissue engineering of the esophagus. Semin. Pediatr. Surg. *23*, 127–134. https://doi.org/10.1053/j.sempedsurg.2014.04.003.

Maghsoudlou, P., Georgiades, F., Tyraskis, A., Totonelli, G., Loukogeorgakis, S.P., Orlando, G., Shangaris, P., Lange, P., Delalande, J.M., De Coppi, P., et al. (2013). Preservation of micro-architecture and angiogenic potential in a pulmonary acellular matrix obtained using intermittent intra-tracheal flow of detergent enzymatic treatment. Biomaterials *34*, 6638–6648. https://doi.org/10.1016/j.biomaterials.2013.05.015.

Maughan, E.F., Butler, C.R., Crowley, C., Teoh, G.Z., Hondt, M.D., Hamilton, N.J., Hynds, R.E., Lange, P., Ansari, T., Elliott, M.J., et al. (2017). A comparison of tracheal scaffold strategies for pediatric transplantation in a rabbit model. Laryngoscope *127*, E449–E457. https://doi.org/10.1002/lary.26611.

Meran, L., Massie, I., Campinoti, S., Weston, A.E., Gaifulina, R., Tullie, L., Faull, P., Orford, M., Kucharska, A., Li, V.S.W., et al. (2020). Engineering transplantable jejunal mucosal grafts using patient-derived organoids from children with intestinal failure. Nat. Med. https://doi.org/10.1038/s41591-020-1024-z.

Park, S.Y., Choi, J.W., Park, J.-K., Song, E.H., Park, S.A., Kim, Y.S., Shin, Y.S., and Kim, C.-H. (2016). Tissue-engineered artificial oesophagus patch using three-dimensionally printed polycaprolactone with mesenchymal stem cells: a preliminary report. Interact. Cardiovasc. Thorac. Surg. *22*, 712–717. https://doi.org/10.1093/icvts/ivw048.

Pellegata, A.F., Tedeschi, A.M., and De Coppi, P. (2018). Whole organ tissue vascularization: engineering the tree to develop the fruits. Front. Bioeng. Biotechnol. *6*, 1–13. https://doi.org/10.3389/fbioe.2018.00056.

Poghosyan, T., Sfeir, R., Michaud, L., Bruneval, P., Domet, T., Vanneaux, V., Luong-Nguyen, M., Gaujoux, S., Gottrand, F., Larghero, J., and Cattan, P. (2015). Circumferential esophageal replacement using a tube-shaped tissue-engineered substitute: an experimental study in minipigs. Surgery *158*, 266–277. https://doi.org/10.1016/j.surg.2015.01.020.

Ren, X., Moser, P.T., Gilpin, S.E., Okamoto, T., Wu, T., Tapias, L.F., Mercier, F.E., Xiong, L., Ghawi, R., Ott, H.C., et al. (2015). Engineering pulmonary vasculature in decellularized rat and human lungs. Nat. Biotechnol. *33*, 1097–1102. https://doi.org/10.1038/nbt.3354.

Robey, T.C., Eiselt, P.M., Murphy, H.S., Mooney, D.J., and Weatherly, R.A. (2000). Biodegradable external tracheal stents and their use in a rabbit tracheal reconstruction model. Laryngoscope *110*, 1936–1942. https://doi.org/10.1097/00005537-200011000-00032.

Saito, M., Sakamoto, T., Fujimaki, M., Tsukada, K., Honda, T., and Nozaki, M. (2000). Experimental study of an artificial esophagus using a collagen sponge, a latissimus dorsi muscle flap, and split-thickness skin. Surg. Today *30*, 606–613. https://doi.org/10.1007/s005950070100.

Takeoka, Y., Matsumoto, K., Taniguchi, D., Tsuchiya, T., Machino, R., Moriyama, M., Oyama, S., Tetsuo, T., Taura, Y., and Nagayasu, T. (2019). Regeneration of esophagus using a scaffoldfree biomimetic structure created with biothree-dimensional printing. PLoS One *14*, 1–12. https://doi.org/10.1371/journal.pone.0211339.

Thomas, B., Bhat, K., and Mapara, M. (2012). Rabbit as an animal model for experimental research. Dent. Res. J. *9*, 111. https://doi.org/10.4103/1735-3327.92960.

Totonelli, G., Maghsoudlou, P., Georgiades, F., Garriboli, M., Koshy, K., Turmaine, M., Ashworth, M., Sebire, N.J., Pierro, A., Eaton, S., and De Coppi, P. (2013). Detergent enzymatic treatment for the development of a natural acellular matrix for oesophageal regeneration. Pediatr. Surg. Int. *29*, 87–95. https://doi.org/10.1007/s00383-012-3194-3.

Urbani, L., Camilli, C., Phylactopoulos, D.-E., Crowley, C., Natarajan, D., Scottoni, F., Maghsoudlou, P., McCann, C.J., Urciuolo, A., De Coppi, P., et al. (2018). Multi-stage bioengineering of a layered oesophagus with in vitro expanded muscle and epithelial adult progenitors. Nat. Commun. *9*, 4286. https://doi.org/10.1038/s41467-018-06385-w.

Urbani, L., Maghsoudlou, P., Milan, A., Menikou, M., Hagen, C.K., Totonelli, G., Camilli, C., Eaton, S., Burns, A., Olivo, A., and De Coppi, P. (2017). Long-term cryopreservation of decellularised oesophagi for tissue engineering clinical application. PLoS One *12*, e0179341. https://doi.org/10.1371/journal.pone.0179341.

Williams, D.F. (2019). Challenges with the development of biomaterials for sustainable tissue engineering. Front. Bioeng. Biotechnol. *7*, 1–10. https://doi.org/10.3389/fbioe.2019.00127.

STAR★METHODS

KEY RESOURCES TABLE

REAGENT or RESOURCE	SOURCE	IDENTIFIER
Antibodies		
Rabbit polyclonal anti-Fibronectin	Abcam	Cat# ab2413; RRID:AB_2262874
Mouse monoclonal anti-Collagen I	Abcam	Cat# ab90395; RRID:AB_2049527
Rabbit polyclonal anti-Collagen IV	Abcam	Cat# ab6586; RRID:AB_305584
Rabbit polyclonal anti-Laminin	Abcam	Cat# ab11575; RRID:AB_298179
Rat polyclonal anti-Ki67	eBioscience	Cat# 14-5698-82; RRID:AB_10854564
Goat anti-Rabbit IgG Alexa Fluor™ 594	ThermoFisher	Cat# A-11037; RRID:AB_2534095
Goat anti-Mouse IgG Alexa Fluor™ 594	ThermoFisher	Cat# A-11032; RRID:AB_2534091
Goat anti-Rat IgG Alexa Fluor™ 488	ThermoFisher	Cat# A-11006; RRID:AB_141373
Normal Goat Serum	ThermoFisher	PCN5000
Chemicals, peptides, and recombinant proteins		
Sodium deoxycholate	Sigma Aldrich	30970
DNase I, Bovine Pancreas	Millipore	260913
Paraformaldehyde	Sigma Aldrich	158127
Tissue-Tek® O.C.T. Compound	Sakura Finetek	4583
Triton™ X-100	Sigma Aldrich	X100
Bovine Serum Albumin	Sigma Aldrich	A7030
TRIS buffer saline	Sigma Aldrich	T5912
OmniPur® Methylene Blue, Trihydrate	Sigma Aldrich	6210-OP
Critical commercial assays		
SPECTRA H&E Stains	Leica	3801654
DNeasy Blood & Tissue Kit	Qiagen	69504
QuickZyme Total Collagen Assay kit	QuickZyme Biosciences	QZBtotcol
Glycosaminoglycan Assay Blyscan™	Biocolor	B1000
Experimental models: Organisms/strains		
Male and female pigs *Sus scrofa domesticus*	JSR Genetics Ltd	N/A
Male New Zealand white rabbits *Oryctolagus cuniculus*	Charles River Laboratories	N/A
Software and algorithms		
GraphPad Prism version 6.05	GraphPad Software Inc.	https://www.graphpad.com/
BioRender	BioRender	https://biorender.com/

RESOURCE AVAILABILITY

Lead contact

Further information and requests for resources and reagents should be directed to and will be fulfilled by the lead contact, Prof. Paolo De Coppi (p.decoppi@ucl.ac.uk).

Materials availability

This study did not generate new unique reagents.

Data and code availability

- All data produced in this study are included in the article and its supplemental information, or are available from the lead contact upon request.

- This article does not report original codes.
- Any additional information required to reanalyse the data reported in this paper is available from the lead contact upon request.

EXPERIMENTAL MODEL AND SUBJECT DETAILS

Surgical protocol

The project was registered and licence granted (70/7504) by the UK Home Office in accordance with Animals (Scientific Procedures) Act 1986.

Male New Zealand white rabbits (*Oryctolagus cuniculus*) weighing 3.0–3.5 kg, representative of a term baby, were anaesthetised using a combination of intramuscular ketamine and xylazine and inhaled isoflurane. Anaesthesia was maintained with isoflurane either via a laryngeal mask airway (v-gel®) or with an anaesthetic nose cone.

During all surgeries, a 1.6 cm section of cervical oesophagus was resected and a 2 cm section of decellularised porcine scaffold was then implanted orthotopically and two anastomoses performed using 6.0 PDS over a 6F nasogastric tube (NGT).

During Phases Two and Three, following the oesophageal implantation, a limited upper midline laparotomy was performed, and gastrostomy was inserted using a Stamm gastrostomy technique. The stomach was opened and a 14 French (Fr) malecot silicone tube inserted and secured with a 'purse string' suture (Figure 3A). The stomach was then pexied to the anterior abdominal wall. The 14Fr tube was then tunnelled subcutaneously to a position on the rabbit's neck to avoid the tube being bitten. The tube was flushed with water and the rabbit left overnight without gastrostomy feeding. The following day feeds were started as 3–4 boluses of Oxbow Critical Care Fine Grind rabbit feed reconstituted as per manufacturer instructions. Each feed was followed by 10–15 mL saline flush. Where the tube became blocked, attempts to unblock it were made by boluses of warm saline in a 50 mL syringe. A bioabsorbable PDS BD stent (SX-Ella; 20 × 4 mm) was applied in the scaffold lumen prior to implantation in order to avoid early collapse. For the scaffold vascularisation, the rabbits were shaved and prepared for surgery from neck and down the right side of the abdomen. A long single layer, anterior abdominal wall flap was raised taking care to avoid damage to the vascular pedicle. The flap was then flipped cranially and tunnelled subcutaneously to the neck where the stented scaffold can be wrapped in the flap.

Post operatively, rabbits were given enrofloxacin antibiotic prophylaxis and carprofen and buprenorphine analgesia. Rabbits were offered a blended diet from day 1 post operatively (Oxbow® Critical Care Fine Grind) and were euthanised at humane end points according to license requirements.

METHOD DETAILS

Organ collection and scaffold preparation

Male and female piglets ranging from 1 to 8 day-old (1–2.5 kg, JSR Farms Ltd, UK) were sacrificed, fresh oesophagi were harvested and decellularised with a modified version of the previously described detergent enzymatic treatment (DET) (Maghsoudlou et al., 2013; Totonelli et al., 2013). This protocol is designed to remove immunogenic DNA from the tissue whilst maintaining the extracellular matrix (ECM). Upon surgical isolation, the central segments of the oesophagi (approximately 15 cm in length) were obtained. The lumens were washed three times with a povidone-iodine solution. The organs were cut in 4–5 cm portions and placed in a custom decellularisation chamber (Figure 1A) and tide from the proximal end to a silicon tube matching the luminal size. The tissues were then washed for 48 h with deionised water (DIW) and subjected to 2 DET cycles. Each cycle involved the intraluminal perfusion with 4% sodium deoxycholate (SDC, Sigma Aldrich) at 3 ml min^{-1} at room temperature (RT) for 4 h, followed by overnight DIW rinse, and 2000 Kunitz units of DNase I (Millipore) in Hank's Balanced Saline Solution at 1 ml min^{-1} at room temperature for 3 h, followed by overnight DIW rinse. At the end of the decellularization protocol, the scaffolds were washed for 48 h with DIW and γ-irradiated with a dose of approximately 1.8 kGy within 72 h of process completion. Decellularised oesophagi were subsequently used for implantation into the cervical oesophagus of New Zealand white rabbits.

Histological analysis

Tissue samples were fixed in 4% paraformaldehyde (PFA; Sigma Aldrich) at 4°C for 24 h, then washed in DIW, dehydrated in graded alcohol, embedded in paraffin and sectioned at 5 μm. Tissue sections were stained with Haematoxylin and Eosin (H&E; Leica). Pictures were acquired with a Zeiss Axioplan microscope (Zeiss).

Immunofluorescence

Tissue samples were fixed in 4% PFA at RT for 1 h, washed in PBS, dehydrated in 30% sucrose overnight, O.C.T.-embedded (Sakura Finetek) and frozen with ice-cold isopentane (Sigma Aldrich) then stored at −80°C. 7–10 μm thick sections were cut (Leica cryostat, UK), and slides stored at −20°C. Sections were permeabilised with 0.5% Triton X-100 in PBS for 10 min at room temperature, washed in PBS and blocked with 10% goat serum (ThermoFisher Scientific) containing 1% bovine serum albumin (Sigma Aldrich) in tris buffered saline (TBS, Sigma Aldrich) for 2 h at RT. They were then incubated at 4°C overnight with primary antibodies anti fibronectin (1:100; ab2413 Abcam) collagen I (1:200; ab90395 Abcam), collagen IV (1:200; ab6586 Abcam), laminin (1:200; ab11575 Abcam) or KI67 (1:100; 14-5698-82 eBioscience). Sections were washed twice in 0.025% Triton-X (Sigma Aldrich) in TBS, before being incubated with secondary antibodies for 1 h at RT: goat-anti-rabbit (1:500; a11037 ThermoFisher Scientific), goat-anti-mouse (1:500; a11032 ThermoFisher Scientific) and goat-anti-rat (1:500; a11006 ThermoFischer Scientific). Stained samples were imaged using an Olympus IX70 inverted fluorescence microscope or Hamamatsu Nanozoomer S60 digital slide scanner.

DNA quantification

Approximately 25–50 mg of native or decellularised tissue was finely diced into 1 mm^3 portions using a surgical scalpel. Oesophageal tissue was then dried to a constant mass before proceeding. DNA was extracted using a DNeasy Blood & Tissue Kit (Qiagen) as described in the manufacturer's protocol. Purified DNA was quantified using a NanoDrop 1000 spectrophotometer (ThermoFisher Scientific). Total DNA was normalised to the tissue mass.

ECM component quantification

Native and decellularised samples were prepared as per DNA quantification. The total collagen content was extracted using a QuickZyme Total Collagen Assay kit (QuickZyme Biosciences), in accordance with the manufacturer's protocol. Total sulfated glycosaminoglycan (sGAG) extraction was achieved using the Blyscan™ Sulfated Glycosaminocan Assay kit (Biocolor), as described in the manufacturer's protocol. Absorbance was detected using a Tecan Sunrise (Tecan) or Victor X3 (Perkin Elmer). Total concentration was determined using the standard curve, before being normalised to the tissue mass.

Biomechanical tests

Native samples were assayed <12 h post-scheduling of donor animals. Decellularised tissue was assayed between 1 and 4 weeks after DET. All samples were stored in sterile PBS with A/A (1%) at 4°C.

Longitudinal and circumferentially oriented samples were cut to provide flat specimens, 5 mm by ≥ 15 mm, before measuring thickness in triplicate using a dial thickness gauge (Mitutoyo). Samples were inserted into a zwickiLine testing machine (Zwick/Roell) with 10.00 mm grip separation and submerged in 35–37°C water. Samples were preconditioned with 8 cycles of loading-unloading up to 40% strain at a constant rate of 20 mm min^{-1}, before a failure test was performed with the same constant rate. Young's modulus was interpolated from the loading ramp of the failure test, as in equation below. Stress and strain at break provided the ultimate tensile stress and ultimate strain.

$$E = \frac{\sigma_{0.04} - \sigma_{0.02}}{\varepsilon_{0.04} - \varepsilon_{0.02}}$$

Fluid bolus test

A 5cm long decellularised oesophageal scaffold derived from a 3kg piglet was closed on one end with artery forceps and filled with 10mL of methylthioninium chloride 1% solution in PBS (methylene blue Sigma Aldrich). The scaffold was closed on the other end with another artery forceps and maintained under pressure in suspension over a plate. From this moment, the tissue was filmed for 10 min using time-lapse to assess for the presence of leakage.

Micro-CT scan

The specimen was immersed at room temperature in a solution of 10% formalin (to prevent tissue degradation) and potassium triiodide (I_2KI / Lugol's iodine, to impart tissue contrast), with a total iodine content of 63.25 mg / mL (iodine mass of 2.49×10^{-4} mol mL^{-1}), in a 1:1 ratio for 72 h prior to imaging. Before scanning, the specimen was removed from the iodine solution, rinsed in water to remove excess surface iodine and dried using gauze. The specimen was secured using foam supports, Parafilm M (Bemis) and carbon fibre rods to ensure mechanical stability during micro-CT examination. The tissue was returned to 10% formalin to prevent tissue degradation prior to autopsy examination when needed.

Micro-CT images of the specimen were acquired using an XT H 225 ST microfocus CT scanner (Nikon Metrology) with the multi-metal target set to Tungsten. X-ray energy and beam current settings were 80 kV and 88 μA respectively. Exposure time was 500 ms, with the number of projections optimized for the size of the specimen (number of pixels covered within area of interest x 1.5) and one X-ray frame per projection. Projection images were reconstructed using modified Feldkamp filtered back-projection algorithms with proprietary software (CTPro3D; Nikon Metrology) and post-processed using VG Studio MAX 2.2 (Volume Graphics GmbH). Isotropic voxel size was 17.6 μm.

QUANTIFICATION AND STATISTICAL ANALYSIS

Sample size n refers to the number of independent experiments or biological replicates, shown as circles or triangles, as stated in the figure legends. Data are expressed as mean ± SD. Significance was determined by nonparametric unpaired two-tailed Mann-Whitney *U* test. A p-value of less than 0.05 was considered statistically significant. Statistical analysis was performed using GraphPad Prism 6 (GraphPad Software). Comparative animal survival was evaluated with the Survival Curve function of GraphPad Prism 6 and plotted as Kaplan-Meier survival plot.